Composites Part B 273 (2024) 111258

Contents lists available at ScienceDirect

Composites Part B

journal homepage: www.elsevier.com/locate/compositesb

Surface-activated 3D-printed PEEK implant enhances anti-infection and osteogenesis

Zhaolong Wang [a,1], Zhou Yu [b,1], Zhaoyi Wang [a], Shifen Li [a], Liang Song [a], Tiesong Xu [c], Guocheng Shen [c], Yuchen Wang [b], Tingben Huang [b], Xiaofei Dong [a,d,e,**], Guoli Yang [b,***], Changyou Gao [a,d,e,*]

[a] MOE Key Laboratory of Macromolecular Synthesis and Functionalization, International Research Center for X Polymers, Department of Polymer Science and Engineering, Zhejiang University, Hangzhou, 310058, China
[b] The Affiliated Hospital of Stomatology, School of Stomatology, Zhejiang University School of Medicine, Zhejiang Provincial Clinical Research Center for Oral Diseases, Key Laboratory of Oral Biomedical Research of Zhejiang Province, Cancer Center of Zhejiang University, Hangzhou, 310058, China
[c] Ningbo Cibei Medical Treatment Appliance Co., Ltd., Ningbo, 315000, China
[d] Center for Healthcare Materials, Shaoxing Institute, Zhejiang University, Shaoxing, 312099, China
[e] Dr. Li Dak Sum and Yip Yio Chin Center for Stem Cell and Regenerative Medicine, Zhejiang University, Hangzhou, 310058, China

ARTICLE INFO

Handling Editor: Dr Hao Wang

Keywords:
Polyetheretherketone
Implant
Antibacterial
Hyperbranched poly-L-lysine
Osteointegration

ABSTRACT

With the advantage of remarkable mechanical processing ability without losing its strength, polyetheretherketone (PEEK) based medical devices have been drawing great attention in orthopedic treatments. However, its limited osseointegration capacity and susceptibility to bacterial colonization-induced infections pose a considerable risk of implant failure. Current methods of antimicrobial and osteogenic functionalization frequently exhibit conflicting outcomes. The antimicrobial functionalization of implants usually leads to cytotoxicity and histotoxicity, adversely affecting the connection with surrounding tissues, whereas the osteogenic functionalization may inadvertently promote bacterial adhesion and biofilm development. Therefore, it is highly demanded to endow the PEEK implants with antibacterial and osseointegration properties simultaneously. In this study, 3D-printed PEEK implants were surface modified with hyperbranched poly-L-lysine (HBPL) via physisorption (PEEK-*a*-HBPL) and chemical grafting (PEEK-*g*-HBPL), respectively, which were demonstrated by attenuated total reflection Fourier transform infrared spectroscopy, water contact angle, and X-ray photoelectron spectroscopy. Remarkably, both the PEEK-*a*-HBPL and PEEK-*g*-HBPL exhibited significantly improved antibacterial efficacy against *S. aureus* and *E. coli*, while their osteogenesis ability was not affected but even promoted *in vitro*. In an *in vivo* bone-infection and implantation model in rats, significantly reduced surrounding tissue inflammation and larger new bone formation were observed in both the PEEK-*a*-HBPL and PEEK-*g*-HBPL groups compared to the untreated PEEK group. This comprehensive study lays a foundation for the advancing of organic orthopedic implant materials, offering potential solutions to the pressing issues of osseointegration deficits and implant-related infections.

1. Introduction

Bone fractures represent a widespread form of traumatic injury with a global prevalence, imparting significant distress to patients and posing intricate quandaries to both researchers and orthopedic surgeons [1]. Despite of the accessibility of advanced treatment modalities and comprehensive medical care, notably delayed postoperative healing or nonunion occurs in approximately 10 % of cases [2]. These untoward

* Corresponding author. MOE Key Laboratory of Macromolecular Synthesis and Functionalization, International Research Center for X Polymers, Department of Polymer Science and Engineering, Zhejiang University, Hangzhou, 310027, China.
** Corresponding author. MOE Key Laboratory of Macromolecular Synthesis and Functionalization, International Research Center for X Polymers, Department of Polymer Science and Engineering, Zhejiang University, Hangzhou, 310027, China.
*** Corresponding author.
E-mail addresses: dongx8@zju.edu.cn (X. Dong), guo_li1214@zju.edu.cn (G. Yang), cygao@zju.edu.cn (C. Gao).
[1] These authors contributed equally to this work.

https://doi.org/10.1016/j.compositesb.2024.111258
Received 1 November 2023; Received in revised form 23 January 2024; Accepted 27 January 2024
Available online 1 February 2024
1359-8368/© 2024 Elsevier Ltd. All rights reserved.

consequences lead to protracted convalescence periods and heightened patient distress. It is worth mentioning that the impaired fracture healing is especially conspicuous among certain vulnerable cohorts, encompassing osteoporotic, elderly, and malnourished individuals [3]. In addition to the deficient osseointegration, the implant-associated infections are crucial problems for orthopedic implants. The main cause of infection is the aggregation of bacteria around the implant and the formation of biofilms, which can ultimately lead to implant failure [4]. Especially in cases where patients suffer from diabetes or osteoporosis, mature bacterial biofilms can not only adhere to the surface of the implants but can also penetrate the surrounding tissues and joint cavities, causing more severe osteomyelitis [5]. Therefore, research on the antibacterial and promoting osseointegration abilities of the implant is urgently needed.

Titanium (Ti) and titanium alloys, in particular, have witnessed their extensive utilization over the past few decades in the fabrication of implantable medical devices [6,7], including orthopedic and dental implants [8]. This preference stems from their inherent biocompatibility, and outstanding corrosion resistance. Nonetheless, their widespread adoption has been curtailed in recent times due to their high cost, disparities in mechanical performance relative to human bone, and concerns surrounding potential adverse reactions post-implantation. Polyetheretherketone (PEEK) has attracted escalating attention in the realm of biomedical materials owing to its excellent attributes, encompassing outstanding strength, toughness, thermal stability, resistance to creep deformation, chemical inertness and mechanical properties akin to those of natural bone [9,10]. PEEK has achieved notable success across a diverse categories of medical applications, including artificial knee joints [11], spinal fusion [12] and trauma [13], orthopedic implants [14,15], and dental prosthetics [16–18].

Previous research on functional modification of implants has predominantly concentrated on the isolated performance improvements [19–22]. For instance, rough surface coatings have often been used to augment osteogenic capabilities. The antibacterial strategies have traditionally harnessed agents such as antibiotics, metal ions, nanoparticles, or quaternary ammonium salts, among others [23]. These strategies involve various surface modification techniques such as plasma spraying [24], physical or chemical vapor deposition, and sol-gel processing [25], which beset with limitations such as complicated preparation, elevated cost, and non-negligible toxicological concerns.

Nevertheless, the intrinsic biological inertness of PEEK poses a constraint on its utility in bone regeneration [26]. To address this challenge, surface modification of PEEK materials has emerged as a highly efficacious technique for augmenting osseointegration between PEEK and bone tissue while preserving its outstanding bulk properties [27]. To date, various coating materials especially bioactive molecules such as peptides [28], polymers and proteins [29,30] have been commonly used to modify the PEEK surfaces of implants [31–34]. However, these coating technologies have the disadvantages of complex steps and high costs, thereby constraining their applications. Meanwhile, diverse strategies have been explored to improve the ability of PEEK to fight against microorganisms, such as applying coatings of antibiotics, antimicrobial peptides or polymers, treating with sulfonation and coating with metal nanoparticles. Unfortunately, these treatments cannot avoid excessive residues, which can be cytotoxic, and in most cases, the resultant surface lacks sufficient osteointegration.

In this study, we design and process 3D printed PEEK orthopedic implants. Oxygen plasma is used to endow the PEEK surface with hydrophilic property, which is further physically adsorbed with hyperbranched poly-L-lysine (HBPL) (PEEK-*a*-HBPL), or chemical grafting of HBPL after acrylic acid polymerization (PEEK-*g*-HBPL). HBPL is synthesized through a condensation polymerization reaction, which contains both α-PL and ε-PL units [35,36]. The ε-PL is an edible, non-toxic and biodegradable antimicrobial peptide that is effective against gram-negative and gram-positive bacteria and fungi. Its antimicrobial activity is primarily attributed its adsorption to the surface of microbial membranes, leading to physiological damage to the cells. Currently, it is mainly used as an antimicrobial food additive [37]. The α-PL, by forming electrostatic interactions with the negatively charged cell membranes, can regulate cell adhesion, proliferation and differentiation through non-receptor-mediated cell binding mechanisms [38]. The HBPL molecule possesses both the units of ε-PL and α-PL, endowing its dual biological functions of antibacterial ability and promotion cell adhesion [39,40]. The surface physiochemical properties, cell compatibility and osteogenesis, and antibacterial properties of the PEEK--*a*-HBPL and PEEK-*g*-HBPL are characterized *in vitro*, and their enhancement in bone formation and antiinfection abilities are investigated by using a rat bone infection model *in vivo* (Scheme 1).

2. Materials and methods

2.1. Materials

L-Lysine hydrochloride and potassium hydroxide were purchased from Sinopharm Chemical Reagent Co., Ltd (China). Acrylic acid (AAc), *N*-(3-dimethylaminopropyl)-*N*′-ethyl carbodiimide hydrochloride (EDC), and N-hydroxysuccinimide (NHS) were obtained from Aladdin Co., Ltd (China). Alkaline phosphatase assay kit and Cell counting kit-8 (CCK-8) were bought from Beyotime Biotechnology Co. (Jiangsu, China). Triton-X-100 was purchased from Sigma-Aldrich Co. (Shanghai, China). Fetal bovine serum (FBS, Gibco) and minimum essential medium-α (Zhejiang Senrui Biotechnology Co., Ltd., Zhejiang, China) were used as received. The *S. aureus* strain and *E. coli* strain were purchased from China General Microbiological Culture Collection Center (Beijing, China). Pre-osteoblasts of mouse origin obtained from the American Type Culture Collection (MC3T3-E1 Subclone 14) were used in the experiment. Water was purified by a Milli Q water system (Millipore, USA).

2.2. Preparation of surface-modified PEEK substrates

PEEK diamonds ($10 \times 10 \times 5$ mm^3), PEEK dishes (inner diameter 12 mm, outer diameter 14.6 mm, thickness 2.5 mm) and PEEK implants (a diameter of 2 mm and a length of 3 mm) were provided by Ningbo Cibei Medical Treatment Appliance Co., Ltd. (Ningbo, China). All the PEEK samples were fabricated by a 3D printing method, followed by polishing and heat-treatment. The detailed procedure is illustrated in Fig. S1, **Video S1** and **Video S2**.

Before performing the plasma treatment, the PEEK samples were first cleaned with acetone, ethanol, and water under ultrasonication to remove any contaminations. The samples were dried with nitrogen, before the plasma treatment was carried out to modify the PEEK surface by Diener electronic ZEPTO-RF-200RIE equipment with a frequency of 60 Hz. O_2 was used as the processing gas with a flow rate of 50 sccm during the plasma treatment. After the PEEK samples were placed in the chamber, it was evacuated by a rotary pump up to a base pressure of 15−10 Torr (1.5 Pa). The RF power supply was then switched on to ignite the RF glow discharge. The PEEK was treated for 300 s under this condition.

Characterization by gel permeation chromatography (Waters 1525/2414, Waters Corporation, American) found the number average molecular weight (Mn) of 5.8 kDa and a polydispersity index (PDI) of 1.24 for the synthesized HBPL [39,40]. The plasma-treated PEEK substrates were incubated in 5 mg/mL HBPL solution at 80 °C for 12 h, allowing HBPL to physically adsorb onto the PEEK surface to obtain the PEEK--*a*-HBPL, which was gently rinsed with water and dried with nitrogen. The plasma-treated PEEK substrates were incubated in 1 M acrylic acid at 80 °C for 12 h. EDC (575 mg) and NHS (345 mg) were added into 5 mg/mL HBPL solution and stirred for 20 min, before the mixture solution was added into the beaker with the PEEK substrates. The reagents were allowed to react at 37 °C in dark while shaking at 100 rpm for 12 h. The HBPL-grafted PEEK samples (PEEK-*g*-HBPL) were gently rinsed with

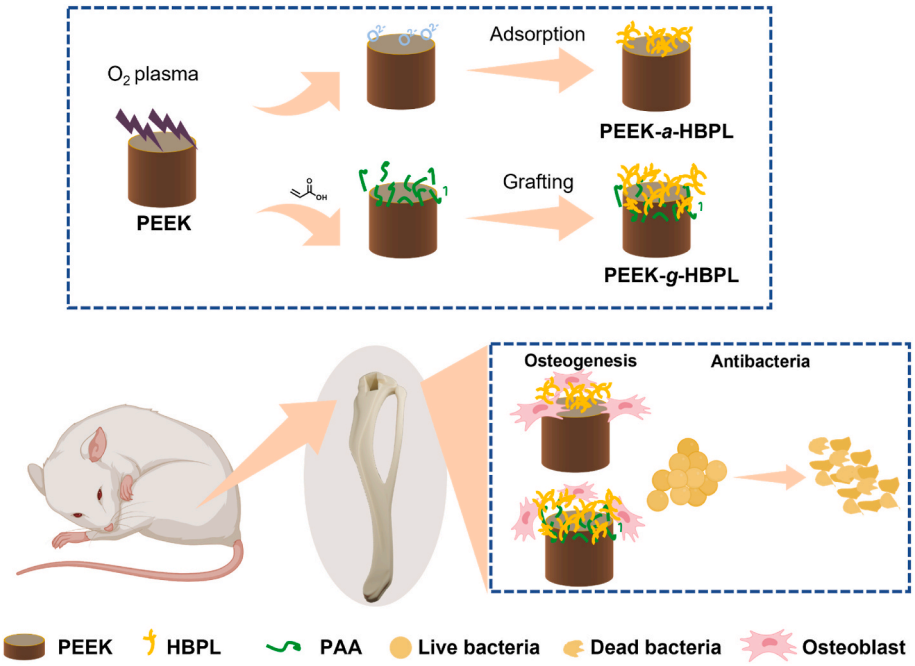

Scheme 1. Scheme of surface modification of polyetheretherketone (PEEK) implants by physical adsorption and chemical grafting of hyperbranched poly-L-lysine (HBPL) to achieve antibacteria and osteogenesis.

water and dried with nitrogen.

2.3. Characterizations of surface-modified PEEK implants

The surface morphology of the samples was scrutinized via scanning electron microscopy (SEM, Hitachi S-4800, Japan) with an accelerating voltage of 15 kV. The SEM images were captured following the gold sputtering on the samples for 30 s. The surface chemistry and elemental analysis were appraised using X-ray photoelectron spectroscopy (XPS, Thermo Scientific K-Alpha, USA). The water contact angle was measured by a water contact measuring machine (Biolin Theta Flex, Switzerland). The chemical composition analysis was performed by means of the attenuated total reflection Fourier transform infrared spectroscopy (ATR-FTIR, Thermo Fisher Scientific Nicolet iS20, American) with a range of 4000–400 cm^{-1}.

2.4. In vitro characterization

2.4.1. Cell culture

The culture of MC3T3-E1 pre-osteoblasts was performed at 37 °C in a humidified atmosphere with 5 % CO_2, using α-MEM supplemented with 10 % FBS, 100 U/mL penicillin and 100 μg/mL streptomycin. The medium was refreshed every 3 d, and cell passage was conducted once the culture flask reached approximately 80 % confluence.

2.4.2. Cell cytotoxicity and proliferation

The cytotoxicity and proliferation were evaluated by Cell Counting Kit-8 (CCK-8). The PEEK, PEEK-*a*-HBPL and PEEK-*g*-HBPL dishes with an inner diameter of 12 mm, outer diameter of 14.6 mm and thickness of 2.5 mm were soaked in 1 mL α-MEM with 100 U/mL penicillin and 100 μg/mL streptomycin for 24 h at 37 °C to obtain the extracts, respectively. The extracts were used to prepare the complete medium with 10 % FBS. The MC3T3-E1 cells (5×10^3 cells/well) were seeded in a 24-well plate for 24 h to allow cell adhesion. Then, the medium was replaced by the medium containing the extracts. After being cultured for 24 h, the medium was removed. The MC3T3-E1 cells were incubated with 10 % CCK-8 for 2 h, and the absorbance of the medium was measured using a microplate reader (Thermoscientific multiskan sky, American) at 450 nm to calculate the cytotoxicity.

The MC3T3-E1 cells (2×10^4 cells/well) were seeded on the surface of the PEEK, PEEK-*a*-HBPL and PEEK-*g*-HBPL specimens in a 24-well plate with α-MEM. After culture for 1, 2 and 3 d, the cells were incubated for 2 h in 10 % CCK-8 to characterize the cell proliferation.

2.4.3. Cell morphology

The interaction between substrates and cells was characterized by SEM. The MC3T3-E1 cells were incubated on the substrates at a density of 2×10^4 cells/well for 1d. The cells were fixed with a 2 % paraformaldehyde/2.5 % glutaraldehyde PBS solution, and then dehydrated. The ethanol gradient method was used to immerse the sample in solutions of varying ethanol concentrations (30 %, 50 %, 70 %, 80 %, 90 %, and 100 % ethanol in water by volume), each for 15 min, with the final step repeated twice. The exchange of solutions was facilitated using gradient tertiary butanol (a mixture of tertiary butanol and ethanol in varying volumes: 30 %, 50 %, 70 %, 90 %, and 100 %), each for 15 min. Afterwards, all of the specimens were subjected to freeze-drying process and coated with a layer of gold in preparation for SEM analysis.

2.4.4. ALP activity

The early osteogenic capacity was assessed through the alkaline phosphatase (ALP) activity of cells. The osteogenic induction medium was comprised of 1 mM sodium β-glycerophosphate, 0.28 mM ascorbic acid, and 1 mM dexamethasone in α-MEM. The MC3T3-E1 cells were incubated on the substrates at a density of 2×10^4 cells/well for 24 h. Following the introduction of the osteogenic induction medium, 1 % Triton-X-100 was utilized to lyse the cells on day 7 and day 14 for a period of 30 min at 4 °C to release the ALP. After the transfer of the medium to a new tube, centrifugation was performed at 5000 rpm and 4 °C for 10 min to obtain the supernatant. According to the manufacturer's instructions, the ALP activity Test Kit (Biyuntian Biotechnology Co., Ltd.) and the Detergent Compatible Bradford Protein Assay Kit (Biyuntian Biotechnology Co., Ltd.) were utilized to test the ALP activity and total protein level, respectively. The final alkaline phosphatase activity was expressed as the number of moles of produced *p*-nitrophenol divided by the time of incubation and amount of protein, and the unit was mmol/min/mg protein.

2.4.5. Extracellular matrix mineralization

The mineralization of the extracellular matrix was assessed by using alizarin red staining. Upon the completion of the osteogenic induction culture for 14 and 21 d, the cells were washed with PBS and fixed with 4 % paraformaldehyde for 1 h, and then rinsed with PBS for 3 times. 200 μL of 0.2 % Alizarin Red S solution (pH = 8.3) was added to each well. Following a 30 min incubation for staining and washing twice, the samples were examined using a stereomicroscope (ZEISS HAL 100, Germany). In order to perform quantitative analysis, a solution containing 10 % (w/w) hexadecylpyridinium chloride in a 10 mM monosodium phosphate solution was used to dissolve the pigments. The optical density was measured at 562 nm via a spectrophotometric microplate reader.

2.5. Antibacterial performance in vitro

2.5.1. Bacterial culture

Representative Staphylococcus aureus (*S. aureus*, ATCC25923) and Escherichia coli (*E. coli*, ATCC25922) were chosen to serve as gram-positive and gram-negative bacteria models. Under a consistent shaking condition (220 rpm) and at a temperature of 37 °C, the experiments were carried out in LB medium.

2.5.2. Bacterial morphology

The morphology was observed via FE-SEM to assess the adherence and diffusion of bacteria on the PEEK, PEEK-*a*-HBPL and PEEK-*g*-HBPL samples. The samples were incubated in a 24-well plate with 200 μL of bacterial suspension (1×10^6 CFU/mL) at 37 °C for 4 h. After removal of the medium, the samples were rinsed with PBS for 3 times. Subsequently, the bacteria on different surfaces were fixed with 4 % paraformaldehyde at 25 °C for 90 min. The samples were then dehydrated through a gradient of ethanol (30 %, 50 %, 70 %, 80 %, 90 % and 100 % v/v), each for 15 min. All of the specimens were subjected to freeze-drying and coated with a layer of gold or SEM analysis.

2.5.3. Antibacterial rates by the spreading plate method

A concentration of 1×10^6 CFU/mL of both *S. aureus* and *E. coli* in LB medium was prepared. Each substrate was transferred to a 24-well plate. A volume of 50 μL of bacterial suspension was applied to each sample surface, and any spaces between the wells surrounding the samples were filled with PBS. Following an incubation period of 4 h at a temperature of 37 °C, 150 μL of PBS was introduced onto the surface of each sample. The bacterial suspension and samples were both gathered and then moved to a 50 mL tube, and subjected to ultrasonication (40 W) for 5 min to dislodge the adherent bacteria. To evaluate the bacterial growth, 100 μL of a diluted suspension of 100 times was placed onto sterile agar plates, which were incubated for an additional 16 h. Following the incubation, images of the agar plates were captured, and the number of colony-forming units (CFUs) were counted. The antibacterial rate was determined by the following formula:

$$\text{Antibacterial rate } (\%) = (\text{C} - \text{E}) / \text{C} \times 100\%$$

where *C* and *E* denote the bacterial colony counts (CFU per sample) for the control group (untreated PEEK sample) and the experimental group, respectively.

2.6. In vivo experiments

All the animal experiments were reviewed and approved by the Institutional Animal Care and Use Committee of Zhejiang University (ZJU20230365). The surgical procedures adhered to the guidelines set forth for animal experimentation research reports (ARRIVE guidelines).

2.6.1. Bone-implant osseointegration in an infected model

Thirty-six Male Sprague-Dawley (SD) rats (body weight 200–300 g) were randomly divided into three equally sized groups: PEEK, PEEK-*a*-HBPL, and PEEK-*g*-HBPL. Briefly, the rats were anesthetized with 2 % pentobarbital sodium (0.2 mL/100 g) through intraperitoneal injection. After shaving the hair around the knee joints, disinfection, injection of lidocaine locally and incision, a cylindrical hole with 2 mm diameter and 3 mm depth was prepared in the medial aspect of the rat distal tibia using a dental drill. One of the PEEK, PEEK-*a*-HBPL, PEEK-*g*-HBPL samples was placed into one cavity. In order to create the infected model, 10 μL *S. aureus* (1×10^5 CFU/mL) was meticulously and gradually inserted into the hole via injection before sample insertion. Finally, the muscle and skin were closed with 4–0 sutures.

2.6.2. In vivo antibacterial and anti-inflammation evaluation

At 3 d after surgery, the blood samples of 18 rats were collected for the biochemical analysis to assess the hepatorenal toxicity. After euthanizing the rats, the implants and their tibias were harvested for further investigations. The implant samples were ultrasonicated for 5 min in 2 mL PBS to isolate the bacteria. The isolated bacteria were diluted and cultured on the sterile brain heart infusion agar plates. After incubation at 37 °C for 1 d, the numbers of bacterial colony were measured. The collected bone specimens were fixed in 4 % paraformaldehyde (PFA), and were decalcified in 10 % ethylene diamine tetraacetic acid (EDTA). After embedded in paraffin, the sections were stained with hematoxylin and eosin (HE) and CD68 anti-body (Boster). The Image Pro Plus software was adopted to analyze the percentages of CD68 positive area.

2.6.3. Micro-CT analysis

After 4 and 8 w surgery, the tibias were collected and fixed in 4 % PFA. The Micro-CT (U-CT-XUHR, Milabs) was applied to scan the bone specimens. The three-dimensional structure of the newly formed bone on the peri-implant region was rebuilt using software. The bone volume to tissue volume (BV/TV), bone mineral density (BMD) and trabecular thickness (Tb.Sp) were further quantitatively evaluated.

2.6.4. Histopathological evaluation

The collected bone specimens were fixed in 4 % PFA, and were decalcified in 10 % EDTA. After embedded in paraffin, the sections were stained with Giemsa, HE, and Masson's trichrome [41–43]. The stained sections were observed and imaged using an optical microscope (Olympus BX53, Japan).

2.6.5. Gait analysis

After 4 w survey, the motor function of rats was measured by the CatWalk XT system (Noldus Information Technology). The footprints were captured and converted to intensity for further analysis.

2.6.6. Statistical analysis

The means ± standard deviation (SD) of data collected from a minimum of three independent experiments are presented, and analyzed through one-way analysis of variance (ANOVA) utilizing Prism software. To guarantee a suitable sample size for statistical analysis in the *in vivo* trials, six mice were assigned to each group. Significant difference levels were set as $^*P < 0.05$, $^{**}P < 0.01$ and $^{***}P < 0.001$ between the selected groups, and *ns* represents no significant difference.

3. Results and discussion

3.1. Surface modification of PEEK

PEEK has been widely used for manufacturing implants used in trauma, orthopedic, and spinal fields since its commercialization in the 1980s. Numerous studies have confirmed its robust mechanical properties in orthopedic implants [44–46]. While many coatings such as calcium phosphate [47], bioactive small molecules [47], hydroxyapatite and titanium [48] have been applied to PEEK surfaces to enhance its

tissue interaction, the surface-modified materials still face many challenges such as susceptibility to degradation, complex and time-consuming chemical steps, and poor adhesion to the substrate, which limit their clinical application [10].To endow the bioactive properties, we developed a feasible method for preparing PEEK implants by activating the 3D-printed PEEK surface with O_2 plasma to enrich the surface with oxygen negative ions. Then physisorption (PEEK-*a*-HBPL) and chemical grafting (PEEK-*g*-HBPL) strategies were employed to introduce HBPL onto the PEEK surface stably.

The oxygen plasma chemically etches the surface by combining excited oxygen with carbon or hydrogen atoms to produce CO_x and H_2O species, respectively [49]. The HBPL interacts with the PEEK surface by electrostatic interaction to form a coating. Another method is grafting of polyacrylic acid (PAA) onto the PEEK surface [50], which can be used to covalently graft HBPL by EDC/NHS reaction [51]. The ATR-FTIR spectra identify the changes of chemical groups on the PEEK-*a*-HBPL and PEEK-*g*-HBPL sample surfaces (Fig. 1a). The peak representing the N–H was observed at 3254 cm^{-1} (marked by the dashed line), indicating the presence of HBPL on the modified PEEK surfaces. The peak at 1706 cm^{-1} represents the C═O (marked by the red arrow) stretching vibration of the amide group, which was unique for the PEEK-*g*-HBPL, and was absent in the PEEK-*a*-HBPL. In Fig. 1b, the N 1s signal with a binding energy of 399.08 eV was observed on the surfaces of the PEEK-*a*-HBPL and PEEK-*g*-HBPL, indicating that HBPL was successfully loaded onto the samples. The quantification detection in Table 1 shows that the N atomic percentages on the surfaces of the PEEK-*a*-HBPL and PEEK-*g*-HBPL were 19.57 % and 9.33 %, respectively. The results of XPS spectroscopy show that the HBPL coating was successful in bio-modifying the PEEK surface, which would play a key role in improving cell behavior. The XPS results further substantiate the presence of HBPL on the modified PEEK. After incubating the surface-modified implants in PBS for 7 d, the amount of N element detected by XPS (Fig. S5) showed no significant change on the PEEK-*g*-HBPL, but decreased remarkably on the PEEK-*a*-HBPL. These results suggest that the covalently immobilized HBPL molecules are robust and highly stable, whereas the electrostatically adsorbed ones are partially desorbed.

The wetting property reflects the change of surface composition of the material surface to some extent. Fig. 1c shows that after O_2 plasma treatment and grafting of PAA, the water contact angle decreased from 76° to 48°. The adsorption of HBPL further enhanced the surface hydrophilicity, resulting a decrease of contact angle to 32°. By contrast, the covalent grafting resulted in a slight larger contact angle with a value of 43°. The macroscopic appearance and microstructure of the PEEK was not significantly changed after surface modification (Fig. 1d), where the traces of fused deposition printing were visible.

Table 1
Elemental content (atom %) of the samples quantitatively characterized by XPS.

Samples	C 1s	O 1s	N 1s
PEEK	85.3	11.9	**2.81**
PEEK-*a*-HBPL	71.9	8.94	**19.57**
PEEK-*g*-HBPL	82.88	7.79	**9.33**

These characterizations demonstrate the successful modification of PEEK substrates with HBPL achieved through either physical or chemical bonds, among which the PEEK-*a*-HBPL possesses a larger amount of HBPL compared to the PEEK-*g*-HBPL likely due to the steric hindrance for surface grafting.

3.2. Antibacterial performance in vitro

Exposed orthopedic wounds are highly susceptible to bacterial infection, which is considered as the main cause of the failure of implant surgery. The implants with antibacterial activity can help prevent surgical site infections. Therefore, the demand of functional implants with antibacterial ability has been increasing in recent years [52]. In this study, *E. coli* and *S. aureus* were chosen to evaluate the antibacterial performance by investigating the number of bacterial colonies in the suspension and their morphology after incubation with different samples. The *S. aureus* is typically spherical with a grape bunch-like distribution in dense areas, while the *E. coli* is a slender rod-shaped bacterium. The *S. aureus* and *E. coli* remained intact on the surfaces of PEEK (Fig. 2a). By contrast, the structures of both bacteria were damaged on the surface with HBPL, where the *S. aureus* showed obvious folds with crumpled and incomplete cell membranes, and the *E. coli* disruption was more drastic. The intracellular contents have been leached away. By the plate spreading method the antimicrobial rate was quantitatively analyzed (Fig. 2b). The numbers of colonies of both the *S. aureus* and *E. coli* on the plates of the PEEK-*a*-HBPL and PEEK-*g*-HBPL groups were very significantly reduced than that of the pure PEEK group. Quantitative data for *S. aureus* (Fig. 2c) and *E. coli* (Fig. 2d) show that the PEEK-*a*-HBPL substrate exhibited 100 % antimicrobial activity against both types of bacteria, whereas the PEEK-*g*-HBPL had an antibacterial activity against *S. aureus* and *E. coli* of 99.6 % and 99.2 % after 4 h

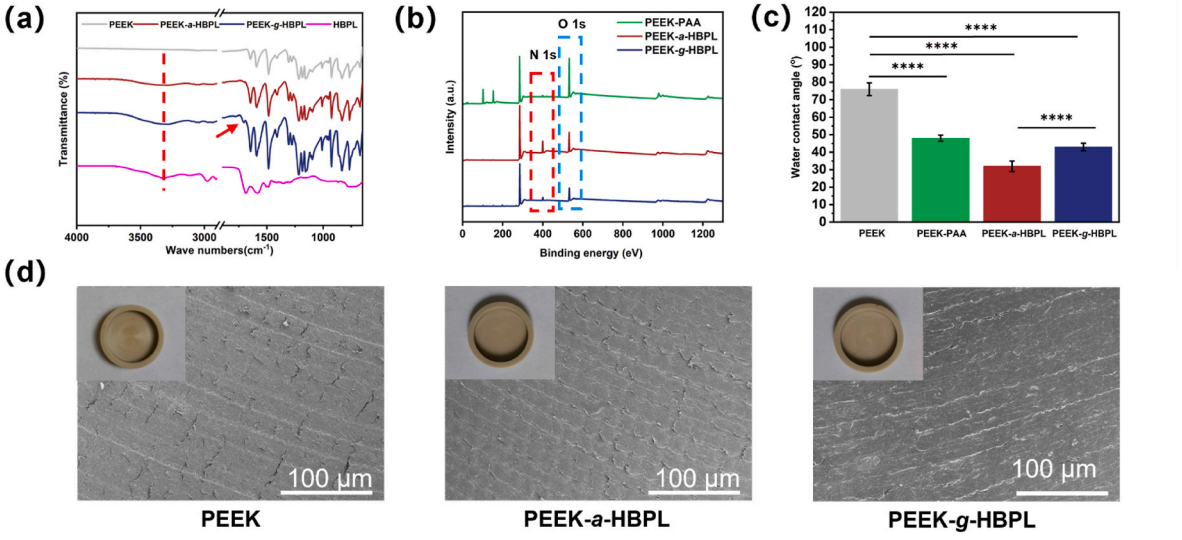

Fig. 1. Preparation and characterization of surface-modified PEEK. (**a**) ATR-FTIR spectra, (**b**) XPS spectra, (**c**) water contact angles, and (**d**) SEM images (inset, photos) of different samples as noted. ****P < 0.0001.

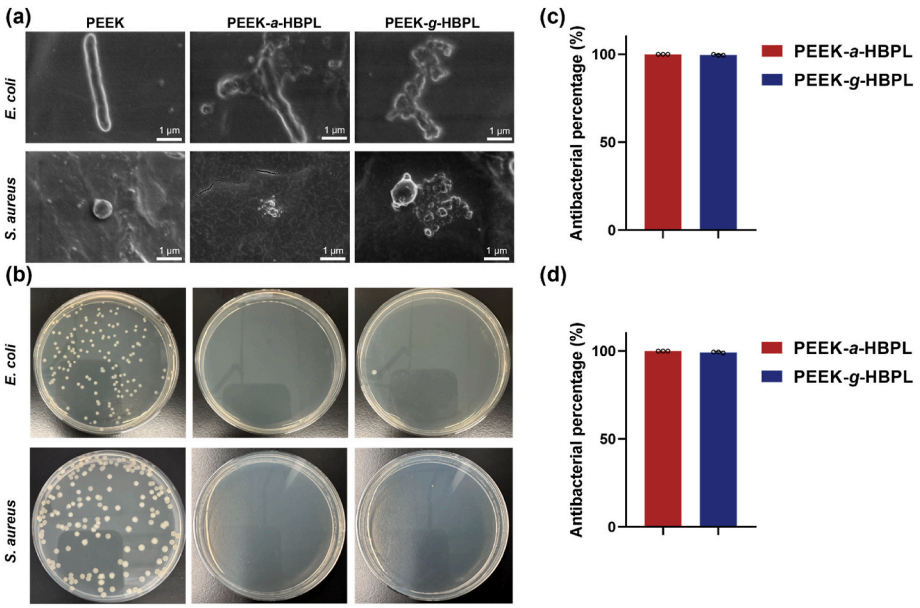

Fig. 2. Antibacterial assessment *in vitro*. (**a**) After incubation for 4 h, the initial morphology of adherent *S. aureus* and *E. coli* on varying substrates was assessed using scanning electron microscopy (SEM). (**b**) Using the spreading plate method, the *S. aureus* and *E. coli* colonies were evaluated. The quantities of *S. aureus* (**c**) and *E. coli* (**d**) colonies were then normalized to that of the corresponding PEEK surface, n = 3.

incubation, respectively.

3.3. In vitro cytocompatibility assays

The morphology of the MC3T3-E1 cells was observed by SEM after 1 d culture (Fig. 3a). Much larger cell spreading regions were shown on

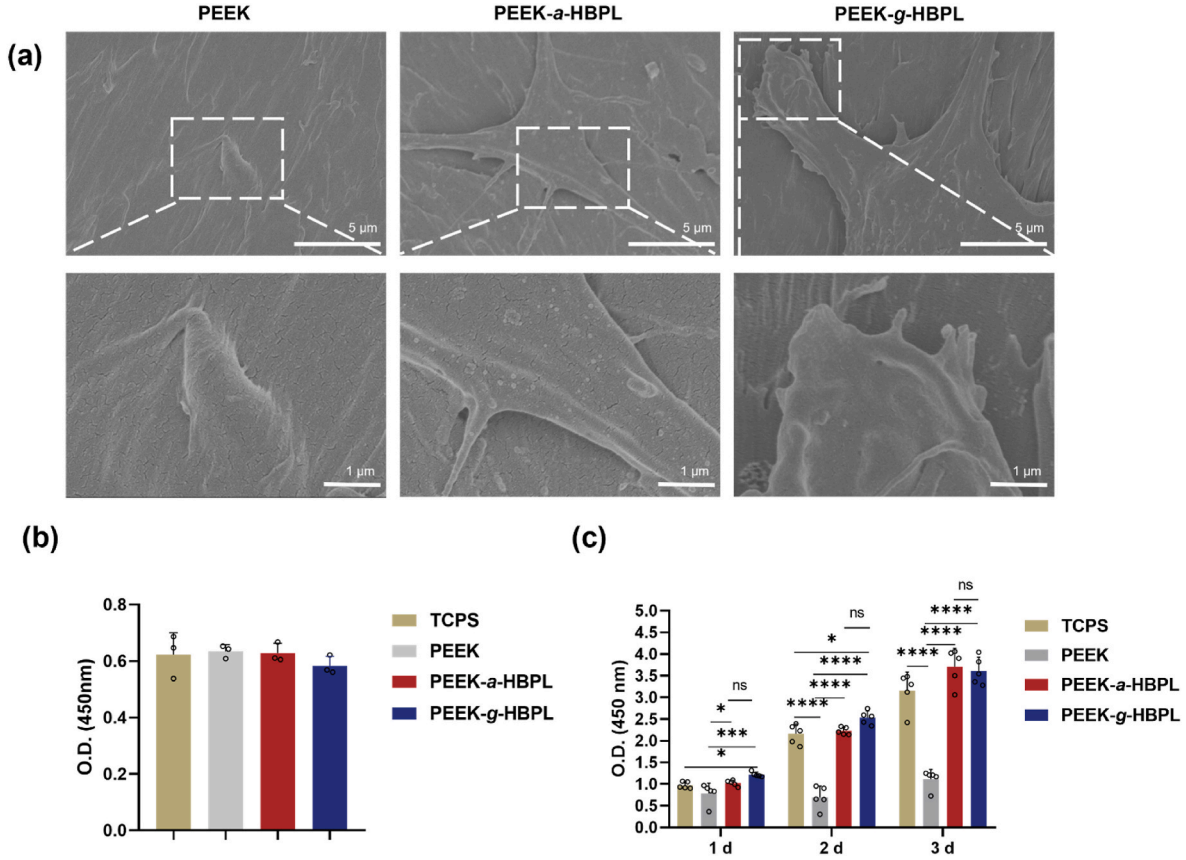

Fig. 3. Cytocompatibility evaluation *in vitro*. (**a**) SEM images showing the cell morphology after being cultured for 24 h. (**b**) Cell viability (expressed as O.D.) estimated by CCK-8 assay, n = 5. (**c**) Relative viability of MC3T3-E1 cells being co-cultured for 24 h with the extracts from PEEK, PEEK-*a*-HBPL and PEEK-*g*-HBPL, respectively. Data are expressed as means ± SD. ns: $P > 0.05$; *$P < 0.05$, ***$P < 0.001$ and ****$P < 0.0001$.

the PEEK-*a*-HBPL and PEEK-*g*-HBPL groups with plenty cell filamentous pseudopods, indicating that the HBPL coating facilitated cell adhesion. Fig. 3b shows that along with the prolongation of culture time, the cell viability on the PEEK-*a*-HBPL and PEEK-*g*-HBPL groups increased much faster than that on the control PEEK, with a value even larger than that on the control group of tissue culture polystyrene substrate (TCPS). No significant difference was found between the PEEK-*a*-HBPL and PEEK-*g*-HBPL groups.

On the other hand, the viability of the MC3T3-E1 cells (Fig. 3c) co-cultured with the extracts of the PEEK-*a*-HBPL and PEEK-*g*-HBPL groups had no significant difference compared with the PEEK group, suggesting neglectable cytotoxicity and thus ensuring their safe implantation *in vivo*.

In summary, the surface modification of HBPL can promote the proliferation of MC3T3-E1 cells, enhancing the cytocompatibility of the PEEK surface without noticeable cytotoxicity. This feature, together with the good antibacterial performance, ensures the reasonable exploration *in vivo* shown below.

3.4. *In vitro* osteogenic potential

The enzymatic activity of ALP is a significant indicator of early osteoblastic differentiation as it governs both cell mineralization and osteogenic differentiation [53]. The osteogenic capability of surface-modified PEEK substrates was evaluated by measuring the ALP activity and calcium deposition amount. As shown in Fig. 4a, the ALP activity of the PEEK-*a*-HBPL, especially the PEEK-*g*-HBPL was upregulated more significantly compared with the PEEK along with the prolongation of culture time from 7 d to 14 d. The higher ALP activity of the HBPL-modified PEEK was consistent with its better cell adhesion and cytoviability, which help the MC3T3-E1 cells turn into the early differentiation stage and expression of ALP.

To evaluate the osteogenic potential of the HBPL coating, calcium deposition, which serves as a late-stage osteogenic marker [54], was also assessed (Fig. 4b). Compared to the PEEK group, a greater number of vivid and red calcium nodules were observed on the surface of the PEEK-*g*-HBPL group at 21 d. The HBPL on the PEEK-*a*-HBPL surface should be less stable in liquid environment for a long period of time due to its physical adsorption nature. The quantification detection also confirmed that the cells on the PEEK-*g*-HBPL produced largest amount of calcium nodules among all the groups, whereas no significant difference was found between the PEEK-*a*-HBPL and PEEK groups (Fig. 4c). The gene expressions of early-stage osteogenic markers such as osteocalcin (OCN), bone morphogenetic protein-2 (BMP2), runt-related transcription factor 2 (Runx2), and osterix (Sp7) were generally higher for cells being cultured for 7 and 14 d on the HBPL-modified surfaces than the pure PEEK surface (Fig. S4). The exact patterns were consistent with ALP activity and calcium deposition (Fig. 4). In particular, the PEEK-*g*-HBPL group was more effective than the PEEK-*a*-HBPL in promoting the osteogenic differentiation, due to the good stability of grafted HBPL over the physically adsorbed ones which could be partially washed off during the replacement of cell culture medium *in vitro*. These results suggest that the HBPL-modified surfaces, especially the PEEK-*g*-HBPL, had excellent *in vitro* osteoinductive ability, and could significantly promote mid to late-stage osteogenic differentiation compared to the PEEK substrate.

Our results show that the HBPL-functionalized PEEK substrates have excellent bactericidal ability and promote osteogenic differentiation of osteoblasts. The antibacterial rates against both *S. aureus* and *E. coli*, representing typical Gram-positive and Gram-negative bacteria are 100 % approximately. The antibacterial mechanism of HBPL has been explored in our previous studies [40]. The high antibacterial ability of

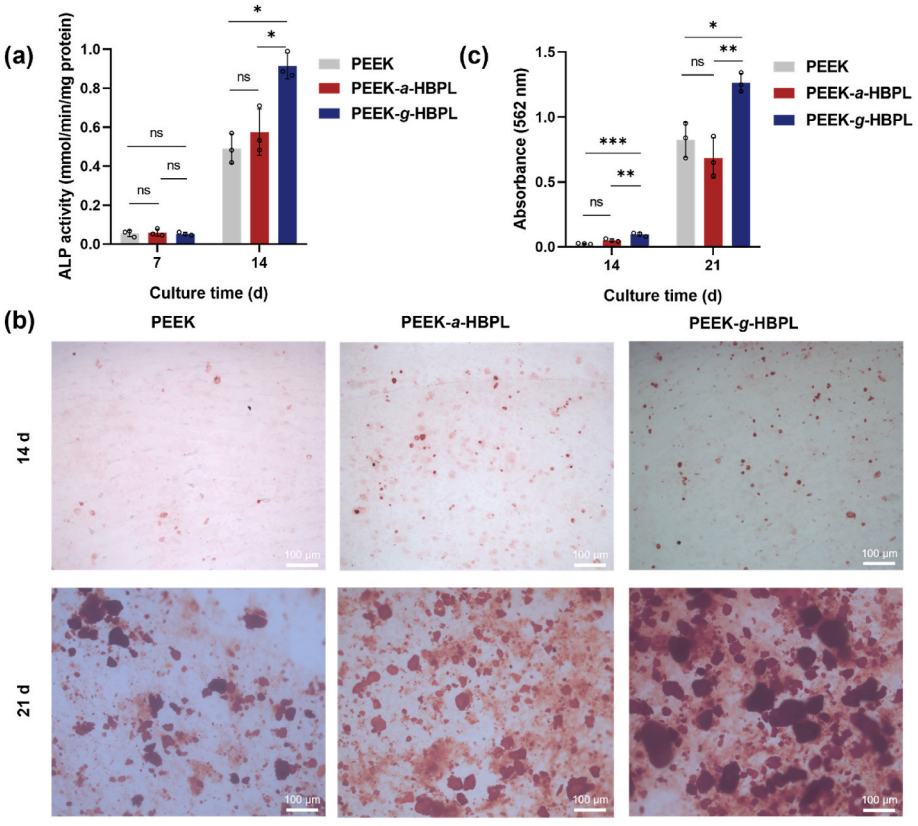

Fig. 4. Osteogenesis ability evaluation *in vitro*. (**a**) ALP activity of the MC3T3-E1 cells was measured after being cultured on different samples for 7 d and 14 d, n = 3. (**b**) Alizarin Red S staining images after MC3T3-E1 cells were cultured for 14 d and 21 d on different samples, n = 3. (**c**) Quantitative analysis of Alizarin Red S staining, n = 3. Data are expressed as means ± SD. ns: $P > 0.05$; *$P < 0.05$, **$P < 0.01$ and ***$P < 0.001$. (For interpretation of the references to colour in this figure legend, the reader is referred to the Web version of this article.)

HBPL is different from most antibiotics and toxic metal ions such as Zn^{2+}, Cu^{2+} and Ag^{+} [55,56]. The bacteria co-cultured with HBPL solution leads to the upregulation of oxidative stress and intracellular ROS level, which affect the expression of genes related to oxidative stress and DNA damage. The HBPL in PEEK-*a*-HBPL group would be partially detached to interact with bacteria around the tissue, leading to bacterial membrane rupture and DNA damage and thereby bacterial death. Therefore, the PEEK-*a*-HBPL group achieved a better antibacterial effect [40]. Moreover, in addition to its strong antibacterial activity against pathogenic bacteria, the PEEK-*g*-HBPL substrate exhibits better cytocompatibility, which promotes the adhesion, proliferation and differentiation of MC3T3-E1 cells.

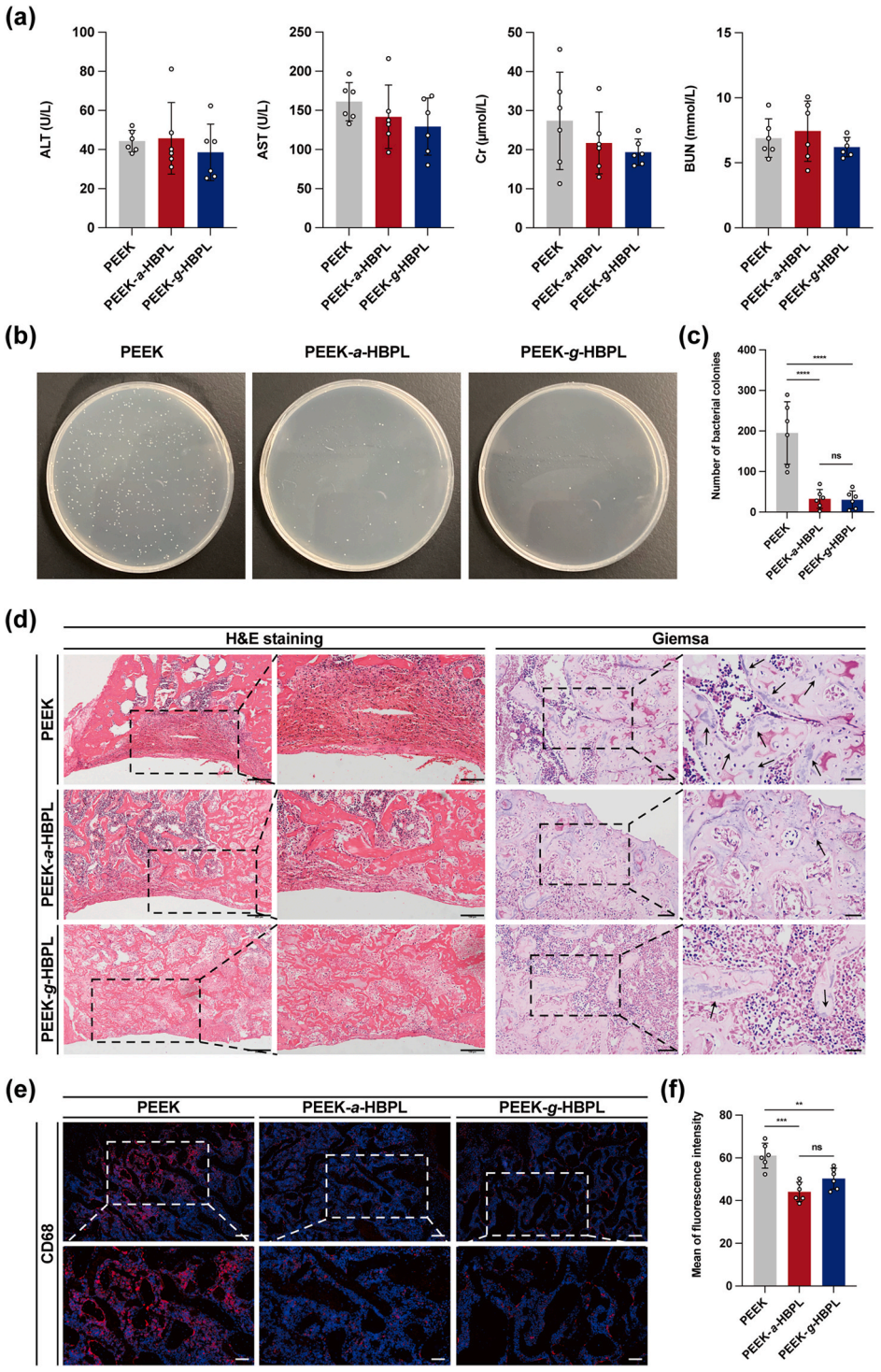

Fig. 5. Assessment of biosafety, antibacterial and anti-inflammatory properties *in vivo*. (**a**) Quantitative analysis of serum ALT, AST, Cr and BUN post-implantation for 3 d. (**b**) Representative images of *S. aureus* colonies characterized by a spread plate method, and (**c**) quantitative bacterial numbers after post-implantation for 3 d. (**d**) Representative images of H&E and Giemsa staining (black arrows point to bacteria). (**e**) Representative immunochemical staining images and (**f**) quantitative analysis of CD68 positive cells, n = 6. Data are presented as mean ± SD. ns: $P > 0.05$; **$P < 0.01$, ***$P < 0.001$ and ****$P < 0.0001$. The scale bar represents 1 μm.

3.5. Biological safety, antibacterial and osseointegration properties in vivo

Tight integration with bone was essential for the long-term stability of implants. To evaluate the antibacterial and osteointegration properties of the PEEK and surface-modified PEEK samples, we designed the suitable shape and fabricated for *in vivo* implantation through 3D printing. A model of distal-tibia bone defect under infection was established in SD rats (Scheme 1).

The biosafety of all implants was assessed first. Consistent with the *in vitro* experiments, no difference was detected among the three groups in the results of serum biochemical test (Fig. 5a), including alanine aminotransferase (ALT), aspartate aminotransferase (AST), creatinine (Cr) and blood urea nitrogen (BUN) levels, indicating that these implants were suitable for *in vivo* implantation without toxicity and side effects on liver and kidney functions.

Then, the samples collected at 3 d post-surgery were subjected to investigation of antibacterial efficiency and inflammatory response. Giemsa staining was applied to detect the bacterial colonies in the infected bone. As shown in Fig. 5b, the numbers of bacterial colonies in the PEEK-*a*-HBPL and PEEK-*g*-HBPL group were remarkably decreased compared to that in the PEEK group. Meanwhile, the bacterial-counting experiment (Fig. 5c) indicated that almost no bacteria remained in the PEEK-*a*-HBPL and PEEK-*g*-HBPL groups, while a large number of bacteria were still isolated from the PEEK group. In addition, the H&E staining of the PEEK group shows the typical features of infection including extensive lymphocyte and neutrophil infiltrations (Fig. 5d). By contrast, relatively few inflammatory cells were observed in the other two groups. Furthermore, we detected the fluorescence intensity of CD68 (Fig. 5e), which was considered as a typical cell surface marker of inflammatory macrophages. Interestingly, the results show that the distribution of $CD68^{+}$ cells in the PEEK-*a*-HBPL group was the lowest (Fig. 5f). These results demonstrate that the PEEK-*a*-HBPL and PEEK-*g*-HBPL implants exhibited stronger antibacterial capability and could prevent implant-related infection *in vivo*.

To investigate the performances of PEEK and surface-modified PEEK samples on new bone formation and osteointegration under infected conditions *in vivo*, Micro-CT was used to reconstruct 3D images and evaluate the new bone formation in the peri-implant area (Fig. 6a). A large extent of new bone formation around the implants was observed in the PEEK-*a*-HBPL and PEEK-*g*-HBPL groups at 4 w and 8 w post-surgery. This conclusion is further confirmed by the corresponding quantitative results, where the higher BV/TV ratio, BMD, and Tb.Th were achieved in the PEEK-*a*-HBPL and PEEK-*g*-HBPL groups (Fig. 6b). Moreover, the osteointegration ability of the implants was evaluated histologically, where the H&E staining was used to visualize the bone-implant interface (Fig. 6c). Fewer new bones were visualized around the implant thread in the PEEK group, where more collagen-rich bone tissue was formed around the PEEK-*a*-HBPL and PEEK-*g*-HBPL implants. These results demonstrate that both the PEEK-*a*-HBPL and PEEK-*g*-HBPL achieved satisfactory osteointegration in the infected animal model. Taking all the

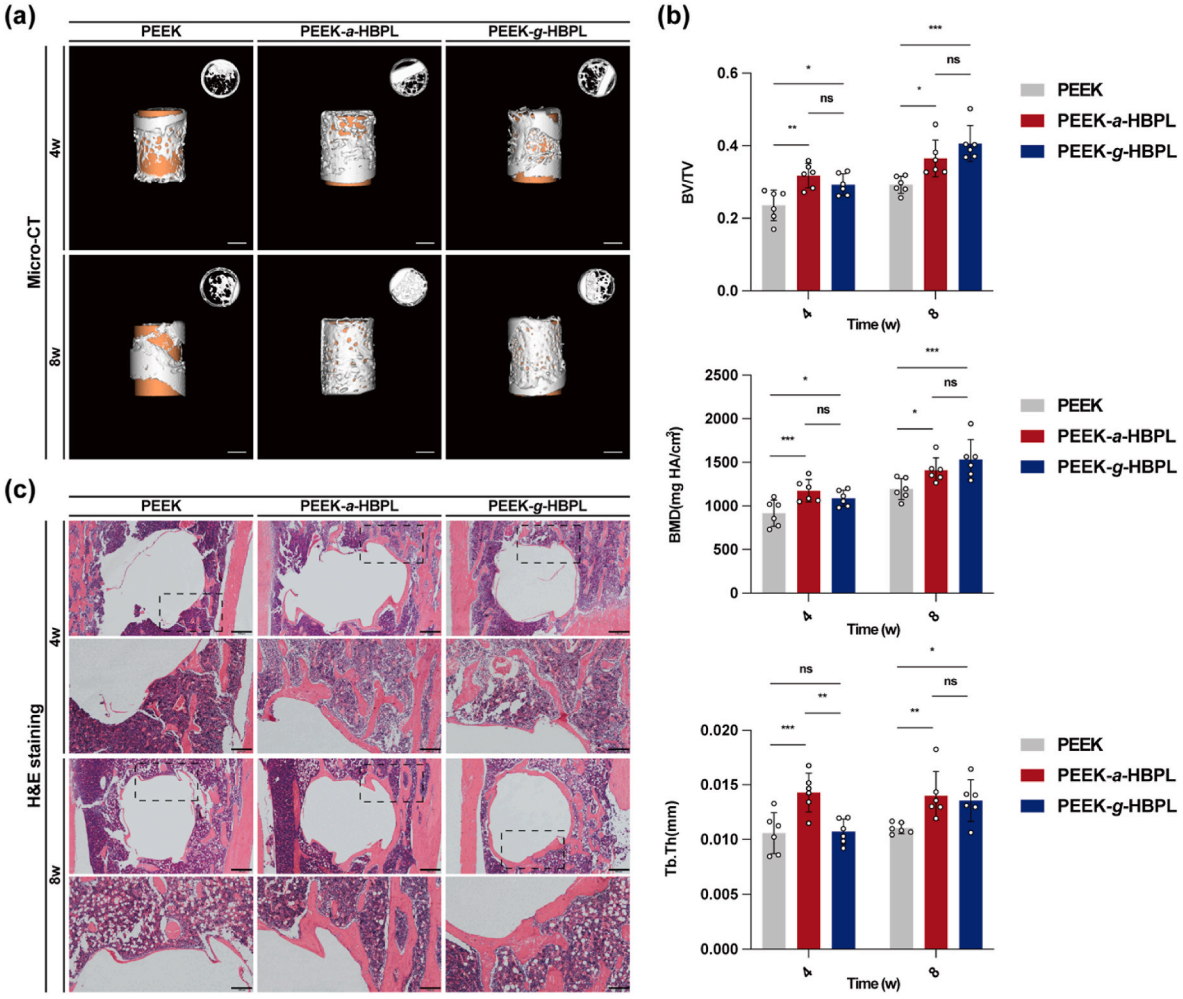

Fig. 6. Assessment of osseointegration in bacteria-infection implantation *in vivo*. (**a**) Representative images of Micro-CT reconstruction after 4 and 8 w post-implantation. (**b**) Quantitative analysis of BV/TV, BMD, and Tb.Th. (**c**) Representative images of H&E staining at 4 and 8 w, n = 6. Data are presented as mean ± SD. ns: $P > 0.05$; *$P < 0.05$, **$P < 0.01$ and ***$P < 0.001$. The scale bar represents 1 μm.

in vitro and *in vivo* experimental results into consideration, the PEEK-*g*-HBPL group showed slightly better osteogenic performance, likely due to the more stable immobilization of HBPL. The good bone formation of the PEEK-*a*-HBPL *in vivo* suggests that the physically adsorbed HBPL can take a similar function on promoting bone formation as the covalently grafted one, likely due to the very limited medium exchange and thereby the sufficient maintenance of HBPL *in situ*.

Consistent with the *in vitro* results, the *in vivo* experiments confirm that the HBPL-modified PEEK implants could well induce new bone formation and integrate with the surrounding bone, exhibit good *in vivo* biocompatibility and osteogenic properties, and had superior antibacterial function. Hence, the HBPL orchestrates the biocompatibility, antibacterial and osteogenic activities simultaneously, which restores the osteogenic microenvironment while clears bacterial infections efficaciously.

3.6. Motor ability of rats

The motor ability of rats was recorded to evaluate the effect of bone formation on moving functions. The Catwalk system captured the footprints of rats and converted to intensity for quantitative evaluation (Fig. 7a and b). According to the print area, the rats in the PEEK-*a*-HBPL showed a better gait pattern with a higher mean intensity (Fig. 7c and d), suggesting that the PEEK-*a*-HBPL improved the walking performance of rats under the infected condition at 4 w. The PEEK-*g*-HBPL could also significantly improve the walking ability. This result is consistent with the larger amount of newly formed bone at the same period of time (Fig. 6).

4. Conclusion

We developed scalable methods for modifying the surface of PEEK implants, encompassing physical adsorption or chemical grafting of HBPL. The PEEK-*a*-HBPL and PEEK-*g*-HBPL had exceptional antibacterial properties both *in vitro* and *in vivo*. The incorporation of HBPL onto PEEK enhanced its hydrophilicity and biocompatibility, and osteogenesis *in vitro* and *in vivo*. Comparatively, the PEEK-*g*-HBPL had greater advantages over PEEK-*a*-HBPL in terms of osteogenic performance, particularly in the promotion of early osteogenic differentiation and late calcium nodule formation. It is highly possible that the discharge of HBPL in the physical adsorption group encourages short-term tissue healing based on the comprehensive outcomes from animal experiments. In regard to the extended osteogenic effects, the PEEK-*g*-HBPL exhibited better performance, potentially due to the enhanced stability of chemically grafted HBPL, enabling sustained effects. This investigation has yielded an antibacterial and osteogenesis PEEK surface, thus holding significant potential as an orthopedic implant for clinical applications.

CRediT authorship contribution statement

Zhaolong Wang: Writing – review & editing, Writing – original draft, Visualization, Validation, Methodology, Investigation, Formal analysis, Data curation, Conceptualization. **Zhou Yu:** Writing – original draft, Validation, Methodology, Investigation, Formal analysis, Data curation, Conceptualization. **Zhaoyi Wang:** Methodology, Investigation. **Shifen Li:** Methodology, Investigation. **Liang Song:** Methodology, Investigation. **Tiesong Xu:** Methodology, Investigation. **Guocheng Shen:** Methodology, Investigation. **Yuchen Wang:** Methodology. **Tingben Huang:** Methodology. **Xiaofei Dong:** Writing – review & editing, Validation, Supervision, Conceptualization. **Guoli Yang:** Writing – review & editing, Supervision, Conceptualization. **Changyou Gao:** Writing – review & editing, Supervision, Resources, Project administration, Funding acquisition, Conceptualization.

Declaration of competing interest

The authors declare that they have no known competing financial

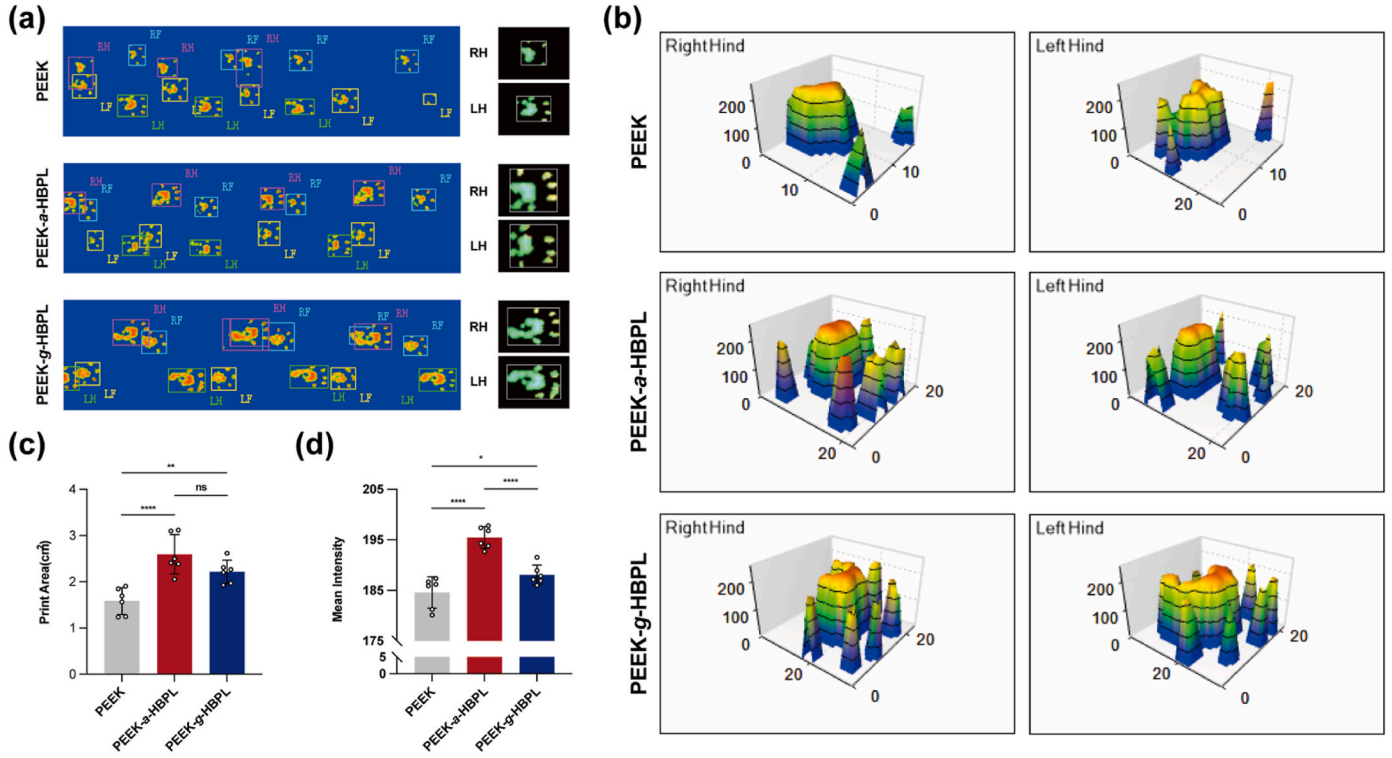

Fig. 7. Gait analysis post implantation for 4 w in the bacteria-infection model. (**a**) Representative images of the Catwalk footprints. (**b**) Measurement of 3D footprint intensities. Quantitative analysis of print area (**c**) and mean intensity (**d**), n = 6. Data are presented as mean ± SD. ns: P > 0.05; *P < 0.05, **P < 0.01 and ****P < 0.0001.

interests or personal relationships that could have appeared to influence the work reported in this paper.

Data availability

Data will be made available on request.

Acknowledgements

This work is financially supported by the Key research and development program of Zhejiang Province (2021C03113), the Natural Science Foundation of Zhejiang Province (LD21E030001), the National Natural Science Foundation of China (U22A20155).

Appendix A. Supplementary data

Supplementary data to this article can be found online at https://doi.org/10.1016/j.compositesb.2024.111258.

References

[1] Winkler T, Sass FA, Duda GN, Schmidt-Bleek K. A review of biomaterials in bone defect healing, remaining shortcomings and future opportunities for bone tissue engineering. Bone & Joint Research 2018;7(3):232–43.
[2] Pfeiffenberger M, Damerau A, Lang A, Buttgereit F, Hoff P, Gaber T. Fracture healing research—shift towards in vitro modeling? Biomedicines Biomedicines 2021;9(7):748.
[3] Lane JM, Russell L, Khan SN. Osteoporosis. Clin Orthop Relat Res 2000;(372):139–50.
[4] Zhou C, Zhou J-T, Sheng C-J, Pranantyo D, Pan Y, Huang X-J. Robust and self-healable antibiofilm multilayer coatings. Chin J Polym Sci 2021;39(4):425–40.
[5] Zhong C, Wu Y, Lin H, Liu R. Advances in the antimicrobial treatment of osteomyelitis. Compos B Eng 2023;249:110428.
[6] Kaur M, Singh K. Review on titanium and titanium based alloys as biomaterials for orthopaedic applications. Mater Sci Eng C 2019;102:844–62.
[7] Zhu H, Zhang H, Chen S, Guan S, Lu W, Zhu H, Ouyang L, Liu X, Mei Y. Fe-NC nanozymes-loaded TiO_2 nanotube arrays endow titanium implants with excellent antioxidant capacity for inflammation inhibition and soft tissue integration. Compos B Eng 2023;267:111054.
[8] Bosshardt DD, Chappuis V, Buser D. Osseointegration of titanium, titanium alloy and zirconia dental implants: current knowledge and open questions. Periodontology 2000 2017;73(1):22–40.
[9] Panayotov IV, Orti V, Cuisinier F, Yachouh J. Polyetheretherketone (PEEK) for medical applications. J Mater Sci Mater Med 2016;27(7):118.
[10] Chen Z, Chen Y, Ding J, Yu L. Blending strategy to modify PEEK-based orthopedic implants. Compos B Eng 2023;250:110427.
[11] Koh YG, Park KM, Lee JA, Nam JH, Lee HY, Kang KT. Total knee arthroplasty application of polyetheretherketone and carbon-fiber-reinforced polyetheretherketone: a review. Mater Sci Eng C 2019;100:70–81.
[12] Seaman S, Kerezoudis P, Bydon M, Torner JC, Hitchon PW. Titanium vs. polyetheretherketone (PEEK) interbody fusion: meta-analysis and review of the literature. J Clin Neurosci : official journal of the Neurosurgical Society of Australasia 2017;44:23–9.
[13] Rendas P, Figueiredo L, Machado C, Mourão A, Vidal C, Soares B. Mechanical performance and bioactivation of 3D-printed PEEK for high-performance implant manufacture: a review. Progress in biomaterials 2023;12(2):89–111.
[14] Zheng Z, Liu P, Zhang X, Jingguo X, Yongjie W, Zou X, Mei X, Zhang S, Zhang S. Strategies to improve bioactive and antibacterial properties of polyetheretherketone (PEEK) for use as orthopedic implants. Materials today. Bio 2022;16:100402.
[15] Wei W, Yang R, Yu Q, Zhao J, Li W. Gallium-niobium nanofiber surface of niobium/PEKK composite with anti-inflammatory, osteogenesis and anti-bacterial effects for facilitating osteoblastic differentiation and ameliorating osteointegration. Compos B Eng 2023;248:110375.
[16] Najeeb S, Zafar MS, Khurshid Z, Siddiqui F. Applications of polyetheretherketone (PEEK) in oral implantology and prosthodontics. Journal of prosthodontic research 2016;60(1):12–9.
[17] Schwitalla A, Müller WD. PEEK dental implants: a review of the literature. J Oral Implantol 2013;39(6):743–9.
[18] Rahmitasari F, Ishida Y, Kurahashi K, Matsuda T, Watanabe M, Ichikawa T. PEEK with reinforced materials and modifications for dental implant applications. Dent J 2017;5(4):35.
[19] Choi S-H, Jang Y-S, Jang J-H, Bae T-S, Lee S-J, Lee M-H. Enhanced antibacterial activity of titanium by surface modification with polydopamine and silver for dental implant application. J Appl Biomater Funct Mater 2019;17(3):2280800019847067.
[20] Al-Shalawi FD, Mohamed Ariff AH, Jung D-W, Mohd Ariffin MK, Seng Kim CL, Brabazon D, Al-Osaimi MO. Biomaterials as implants in the orthopedic field for regenerative medicine: metal versus synthetic polymers. Polymers 2023;15(12):2601.
[21] Wei X, Zhou W, Tang Z, Wu H, Liu Y, Dong H, Wang N, Huang H, Bao S, Shi L, Li X, Zheng Y, Guo Z. Magnesium surface-activated 3D printed porous PEEK scaffolds for in vivo osseointegration by promoting angiogenesis and osteogenesis. Bioact Mater 2023;20:16–28.
[22] Zheng Y, Gao A, Bai J, Liao Q, Wu Y, Zhang W, Guan M, Tong L, Geng D, Zhao X, Chu PK, Wang H. A programmed surface on polyetheretherketone for sequentially dictating osteoimmunomodulation and bone regeneration to achieve ameliorative osseointegration under osteoporotic conditions. Bioact Mater 2022;14:364–76.
[23] Paterson TE, Shi R, Tian J, Harrison CJ, De Sousa Mendes M, Hatton PV, Li Z, Ortega I. Electrospun scaffolds containing silver-doped hydroxyapatite with antimicrobial properties for applications in orthopedic and dental bone surgery. J Funct Biomater 2020;11(3):58.
[24] Chen J, Xie L, Ruan Q, Gao A, Liao Q, Mo S, Lv Y, Tong L, Wang H, Chu PK, Li X. Diamond-like carbon coating and surface grafting of osteoprotegerin and alendronate on polyetheretherketone to ameliorate the mechanical performance and osseointegration simultaneously. Compos B Eng 2022;236:109815.
[25] Xue T, Attarilar S, Liu S, Liu J, Song X, Li L, Zhao B, Tang Y. Surface modification techniques of titanium and its alloys to functionally optimize their biomedical properties: thematic review. Front Bioeng Biotechnol 2020;8:603072.
[26] Ma R, Tang T. Current strategies to improve the bioactivity of PEEK. Int J Mol Sci 2014;15(4):5426–45.
[27] Mo S, Tang K, Liao Q, Xie L, Wu Y, Wang G, Ruan Q, Gao A, Lv Y, Cai K, Tong L, Wu Z, Chu PK, Wang H. Tuning the arrangement of lamellar nanostructures: achieving the dual function of physically killing bacteria and promoting osteogenesis. Mater Horiz 2023;10(3):881–8.
[28] Li M, Bai J, Tao H, Hao L, Yin W, Ren X, Gao A, Li N, Wang M, Fang S, Xu Y, Chen L, Yang H, Wang H, Pan G, Geng D. Rational integration of defense and repair synergy on PEEK osteoimplants via biomimetic peptide clicking strategy. Bioact Mater 2022;8:309–24.
[29] Chen R, Willcox MDP, Ho KKK, Smyth D, Kumar N. Antimicrobial peptide melimine coating for titanium and its in vivo antibacterial activity in rodent subcutaneous infection models. Biomaterials 2016;85:142–51.
[30] Kucharíková S, Gerits E, De Brucker K, Braem A, Ceh K, Majdič G, Španič T, Pogorevc E, Verstraeten N, Tournu H, Delattin N, Impellizzeri F, Erdtmann M, Krona A, Lövenklev M, Knezevic M, Fröhlich M, Vleugels J, Fauvart M, De Silva WJ, Vandamme K, Garcia-Forgas J, Cammue BPA, Michiels J, Van Dijck P, Thevissen K. Covalent immobilization of antimicrobial agents on titanium prevents Staphylococcus aureus and Candida albicans colonization and biofilm formation. J Antimicrob Chemother 2016;71(4):936–45.
[31] Shu R, Sun J, Li B, Gao X, He M, Chan YK, Shi J, Bai D, Yang W, Deng Y. Self-tandem bio-heterojunctions empower orthopedic implants with amplified chemo-photodynamic anti-pathogenic therapy and boosted diabetic osseointegration. Adv Funct Mater 2023;33(27):2214873.
[32] Huang J, Lin S, Bai X, Li W, Zhang R, Miao C, Zhang X, Huang Z, Chen M, Weng S. Decorated polyetheretherketone implants with antibacterial and antioxidative effects through layer-by-layer nanoarchitectonics facilitate diabetic bone integration with infection. ACS Appl Mater Interfaces 2022;14(47):52579–98.
[33] Li N, Bai J, Wang W, Liang X, Zhang W, Li W, Lu L, Xiao L, Xu Y, Wang Z, Zhu C, Zhou J, Geng D. Facile and versatile surface functional polyetheretherketone with enhanced bacteriostasis and osseointegrative capability for implant application. ACS Appl Mater Interfaces 2021;13(50):59731–46.
[34] Zhang S, Feng Z, Hu Y, Zhao D, Guo X, Du F, Wang N, Sun C, Liu C, Liu H. Endowing polyetheretherketone implants with osseointegration properties: in situ construction of patterned nanorod arrays. Small 2022;18(5):2105589.
[35] Scholl M, Nguyen TQ, Bruchmann B, Klok H-A. The thermal polymerization of amino acids revisited; Synthesis and structural characterization of hyperbranched polymers from L-lysine. J Polym Sci Polym Chem 2007;45(23):5494–508.
[36] Zou Y-J, He S-S, Du J-Z. ε-Poly(L-lysine)-based hydrogels with fast-acting and prolonged antibacterial activities. Chin J Polym Sci 2018;36(11):1239–50.
[37] Shima S, Matsuoka H, Iwamoto T, Sakai H. Antimicrobial action of epsilon-poly-L-lysine. J Antibiot 1984;37(11):1449–55.
[38] Yavin E, Yavin Z. Attachment and culture of dissociated cells from rat embryo cerebral hemispheres on polylysine-coated surface. J Cell Biol 1974;62(2):540–6.
[39] Bai J, Zuo X, Feng X, Sun Y, Ge Q, Wang X, Gao C. Dynamic titania nanotube surface achieves UV-triggered charge reversal and enhances cell differentiation. ACS Appl Mater Interfaces 2019;11(40):36939–48.
[40] Yang Z, Xi Y, Bai J, Jiang Z, Wang S, Zhang H, Dai W, Chen C, Gou Z, Yang G, Gao C. Covalent grafting of hyperbranched poly-L-lysine on Ti-based implants achieves dual functions of antibacteria and promoted osteointegration in vivo. Biomaterials 2021;269:120534.
[41] Zhou T, Ran J, Xu P, Shen L, He Y, Ye J, Wu L, Gao C. A hyaluronic acid/platelet-rich plasma hydrogel containing MnO2 nanozymes efficiently alleviates osteoarthritis in vivo. Carbohydr Polym 2022;292:119667.
[42] Wang Z, Xiong H, Zhai Z, Yao Y, Zhou T, Zhang H, Fan C, Gao C. Reactive oxygen species-scavenging nanoparticles coated with chondroitin sulfate protect cartilage against osteoarthritis in vivo. Nano Res 2023;16(2):2786–97.
[43] Wang Z, Cao W, Wu F, Ke X, Wu X, Zhou T, Yang J, Yang G, Zhong C, Gou Z, Gao C. A triphasic biomimetic BMSC-loaded scaffold for osteochondral integrated regeneration in rabbits and pigs. Biomater Sci 2023;11(8):2924–34.
[44] Reddy KUK, Verma PC, Rathi A, Saravanan P. A comprehensive mechanical characterization of as-printed and saliva soaked 3D printed PEEK specimens for low-cost dental implant applications. Mater Today Commun 2023;36:106438.
[45] Wang X, Ma N, Feng L, Shen M, Zhou Y, Zhang X, Huang R, Zhou L, Ji S, Lou Y, Zhu Z. Fabrication of bFGF/polydopamine-loaded PEEK implants for improving soft tissue integration by upregulating Wnt/β-catenin signaling. Heliyon 2023;9(4):e14800.

[46] Wang L, He H, Yang X, Zhang Y, Xiong S, Wang C, Yang X, Chen B, Wang Q. Bimetallic ions regulated PEEK of bone implantation for antibacterial and osteogenic activities. Materials Today Advances 2021;12:100162.
[47] Sunarso, Tsuchiya A, Toita R, Tsuru K, Ishikawa K. Enhanced osseointegration capability of poly(ether ether ketone) via combined phosphate and calcium surface-functionalization. Int J Mol Sci 2020;21(1):198.
[48] Ouldyerou A, Merdji A, Aminallah L, Roy S, Mehboob H, Özcan M. Biomechanical performance of Ti-PEEK dental implants in bone: an in-silico analysis. J Mech Behav Biomed Mater 2022;134:105422.
[49] Chemical Reactions and Equilibrium. In principles of plasma discharges and materials processing. 2005. p. 207–33.
[50] Spyrides SMM, Prado Md, Araujo JRd, SimÃO RA, Bastian FL. Effects of plasma on polyethylene fiber surface for prosthodontic application. J Appl Oral Sci 2015;23 (6):614–22.
[51] Park C, Vo CL-N, Kang T, Oh E, Lee B-J. New method and characterization of self-assembled gelatin–oleic nanoparticles using a desolvation method via carbodiimide/N-hydroxysuccinimide (EDC/NHS) reaction. Eur J Pharm Biopharm 2015;89:365–73.
[52] Li Y, Liu C, Cheng X, Wang J, Pan Y, Liu C, Zhang S, Jian X. PDA-BPs integrated mussel-inspired multifunctional hydrogel coating on PPENK implants for anti-tumor therapy, antibacterial infection and bone regeneration. Bioact Mater 2023; 27:546–59.
[53] Tang Z, Chen H, He H, Ma C. Assays for alkaline phosphatase activity: progress and prospects. TrAC, Trends Anal Chem 2019;113:32–43.
[54] Kolodkin-Gal I, Parsek MR, Patrauchan MA. The roles of calcium signaling and calcium deposition in microbial multicellularity. Trends Microbiol 2023;31(12): 1225–37.
[55] Zhao Q, Yi L, Hu A, Jiang L, Hong L, Dong J. Antibacterial and osteogenic activity of a multifunctional microporous coating codoped with Mg, Cu and F on titanium. J Mater Chem B 2019;7(14):2284–99.
[56] Zhao L, Wang H, Huo K, Cui L, Zhang W, Ni H, Zhang Y, Wu Z, Chu PK. Antibacterial nano-structured titania coating incorporated with silver nanoparticles. Biomaterials 2011;32(24):5706–16.